A compact fiber-optic SHG scanning endomicroscope and its application to visualize cervical remodeling during pregnancy

Yuying Zhang[a,1], Meredith L. Akins[b,c,1], Kartikeya Murari[a], Jiefeng Xi[a], Ming-Jun Li[d], Katherine Luby-Phelps[e], Mala Mahendroo[b,c,2], and Xingde Li[a,2]

[a]Department of Biomedical Engineering, Johns Hopkins University, Baltimore, MD 21205; [b]Department of Obstetrics and Gynecology, [c]Green Center for Reproductive Biology Sciences, and [e]Department of Cell Biology, UT Southwestern Medical Center, Dallas, TX 75390; and [d]Science and Technology Division, Corning Incorporated, Corning, NY 14831

Edited by* David W. Russell, University of Texas Southwestern Medical Center, Dallas, TX, and approved July 2, 2012 (received for review December 28, 2011)

We report the development of an all-fiber-optic scanning endomicroscope capable of high-resolution second harmonic generation (SHG) imaging of biological tissues and demonstrate its utility for monitoring the remodeling of cervical collagen during gestation in mice. The endomicroscope has an overall 2.0 mm diameter and consists of a single customized double-clad fiber, a compact rapid two-dimensional beam scanner, and a miniature compound objective lens for excitation beam delivery, scanning, focusing, and efficient SHG signal collection. Endomicroscopic SHG images of murine cervical tissue sections at different stages of normal pregnancy reveal progressive, quantifiable changes in cervical collagen morphology with resolution similar to that of bench-top SHG microscopy. SHG endomicroscopic imaging of ex vivo murine and human cervical tissues through intact epithelium has also been performed. Our findings demonstrate the feasibility of SHG endomicroscopy technology for staging normal pregnancy, and suggest its potential application as a minimally invasive tool for clinical assessment of abnormal cervical remodeling associated with preterm birth.

nonlinear endomicroscopy | fiber-optic scanning probe | cervical collagen remodeling | parturition

The cervix is a connective tissue-rich structure just caudal to the uterus in female mammals. Appropriate remodeling of the cervix during gestation is an essential component of the birth process (1, 2). The cervix must remain closed during pregnancy to maintain the fetus in the womb, and then open sufficiently to allow passage of the fetus at term. This shift in responsibility requires a massive rearrangement of the cervical connective tissue, in particular fibrillar collagen. Collagen is the main structural protein in the cervix. Animal studies reveal rearrangement of collagen structure is achieved in part by a decline in collagen cross-link formation, a reduction in matricellular proteins that regulate collagen fibrillogenesis, and increased synthesis of the matrix disorganizing molecule, hyaluronan (3, 4). Evidence to support a conservation of these processes in cervical remodeling in women is mounting (5). Abnormal or inappropriately timed cervical remodeling can lead to premature birth.

Preterm birth (PTB), which accounts for 12.7% of all births in the United States, is the second leading cause of infant mortality and often leads to serious morbidity in surviving infants (6). Despite considerable research, the cause of PTB in 50% of cases remains elusive, and diagnostic methods to detect women at risk of PTB are limited (7). Because clinical and animal studies suggest that cervical changes precede the onset of uterine contractility in both term and PTB, premature cervical changes could be indicative of impending PTB (4, 8–10). The progressive structural changes in fibrillar collagens are directly related to cervical rigidity and thus potentially can serve as a diagnostic indicator for women at risk for PTB.

Second harmonic generation (SHG) microscopy is the most effective method for direct noninvasive imaging of collagen type I in biological tissues at submicrometer resolution (11, 12). Collagen I is the most abundant collagen in the cervical matrix. A recent study used SHG microscopy to reveal progressive changes in collagen matrix architecture in mouse cervical tissue sections during normal pregnancy and in one mouse model of PTB (13). This method was able to detect quantifiable changes in cervical collagen earlier than biomechanical changes can be detected. Quantification of these changes by relatively simple metrics showed the progress of collagen matrix remodeling at various stages of normal pregnancy and revealed unexpected insights regarding the mechanism of one mouse PTB model. Application of this emerging technology in the clinic thus holds the promise for significant improvement in assessment and prediction of the risk for preterm birth.

Translation of cervical SHG microscopy for clinical use in vivo represents a formidable engineering challenge, which requires miniaturization of a bench-top microscope down to a small imaging probe applicable for minimally invasive imaging of the cervix. Fiber optics-based miniature and flexible imaging devices such as endoscopes and catheters have established new landscapes for clinical applications of high-resolution optical imaging technologies, including optical coherence tomography (14), confocal imaging (15), and more recently, nonlinear optical imaging (16, 17). Developing a miniature fiber-optic scanning endomicroscope for high-resolution nonlinear imaging (SHG and multiphoton fluorescence) has drawn increasing interest among several research groups including our own (16, 18–23). Since our report of the first prototype scanning fiber-optic two-photon fluorescence endomicroscope (16), we have identified several critical technological challenges and engineering building blocks for developing a high-performance SHG endomicroscopy technology (20, 21). In addition to the challenges in effective excitation pulse delivery, SHG signal collection and miniature beam scanner, one significant challenge for an SHG imaging endomicroscope is the more restrictive demand for low chromatic aberration in the micro-objective lens (21), considering the large wavelength separation between the excitation and emission in SHG imaging (which is typically much larger than the separation in two-photon fluorescence imaging).

Author contributions: Y.Z., M.L.A., M.J.L., K.L.P., M.M., and X.L. designed research; Y.Z. and M.L.A. performed research; Y.Z., M.L.A., K.M, J.X., K.L.P, M.M., and X.L. analyzed data; and Y.Z., M.L.A., K.L.P., M.M., and X.L. wrote the paper.

The authors declare no conflict of interest.

*This Direct Submission article had a prearranged editor.

[1]Y.Z. and M.L.A. contributed equally to this work.

[2]To whom correspondence may be addressed. E-mail: xingde@jhu.edu or mala.mahendroo@utsouthwestern.edu.

This article contains supporting information online at www.pnas.org/lookup/suppl/doi:10.1073/pnas.1121495109/-/DCSupplemental.

www.pnas.org/cgi/doi/10.1073/pnas.1121495109

In this paper, we discuss the technological development of an SHG endomicroscope with improved nonlinear signal collection efficiency and resolution. The performance of the SHG endomicroscope was demonstrated for assessing cervical collagen fiber morphology in the mouse cervix ex vivo and morphological changes in SHG images correlated with established histological findings. Quantitative analyses of endomicroscopic images revealed a progressive increase in collagen fiber size and SHG signal intensity during the course of pregnancy as previously shown by bench-top SHG microscopy (13). Differences in collagen signal were observed very early in pregnancy, allowing the identification of structural aberrations well before changes in biomechanical properties of the tissue could be detected (9, 13). The promise of the endomicroscope for future in vivo studies was further demonstrated by resolving mouse and human cervical collagen fiber morphologies through the intact epithelium. This work provides proof-of-principle that SHG endomicroscopy has potential as a noninvasive method to assess cervical remodeling status during pregnancy, from which PTB-associated risk can potentially be revealed.

Results

Compact SHG Endomicroscope Development. Fig. 1*A* shows a schematic of the distal end of the SHG endomicroscope probe where a single double-clad fiber (DCF) was used for both femtosecond excitation light delivery to and SHG signal collection from the sample. The use of a single DCF (along with other miniature components as described below) helps reduce the overall probe size. The fundamental working principle has been detailed elsewhere (16, 21, 24). In essence, the probe consists of three main parts: (*i*) a four-quadrant piezoelectric (PZT) tube to actuate a fiber cantilever, (*ii*) a single piece of DCF running through and glued to the end of the PZT tube to serve as a cantilever and perform fast two-dimensional beam scanning, and (*iii*) a miniature objective lens at the distal end of the probe to focus the excitation beam and collect the SHG signal. In order to develop a high-performance nonlinear optical imaging endomicroscope, several new advancements have been introduced to the basic design of the endoscope. First, a new customized DCF (Corning Inc.) was developed. The DCF has a single-mode core of a 5.5-μm diameter and a 0.12 numerical aperture (NA) for delivering excitation femtosecond pulses and a large inner-clad of a 185-μm diameter and 0.3 NA for collecting the SHG signal. A photo of the DCF cross-section is shown in Fig. 1*B*. Compared to a commercially available DCF (with an inner clad diameter of 100 μm and an NA of 0.23), the larger inner-clad diameter and higher NA of the customized DCF improves SHG signal collection efficiency by approximately 4.5-fold [i.e., $(185/100)^2 \times (0.3/0.23)$]. In addition, a miniature compound lens with an NA of 0.8 and a working distance of 200 μm in water was utilized. The microlens has super achromatic performance with negligible focal shift between the excitation (800–900 nm) and the SHG signal (400–450 nm). Ray tracing analysis indicates that the maximum focal shift is less than 20 μm between 890 nm (excitation) and 445 nm (SHG emission), which corresponds to a cone with an end diameter of 4.8 μm for the SHG light when focused back to the DCF facet. That is much smaller than the 185-μm signal collection diameter of the DCF. The superb achromatic performance of the micro-objective lens further improved the SHG collection efficiency by more than eightfold when experimentally compared to a commonly used gradient index (GRIN) lens.

The DCF cantilever, tubular PZT actuator and microlens were assembled into a hypodermic tube with an overall dimension of 2 mm × 32 mm (diameter × length). A photograph of the distal end of the endomicroscope is shown in Fig. 1*C*. The small form factor of the endomicroscope also enables its potential integration with other medical instruments for various clinical applications in vivo. The schematic of the entire endomicroscopy system setup is shown in Fig. 1*D*, which includes the femtosecond laser, the dispersion management unit, the scanning endomicroscope, and the SHG signal detection unit. The details about the optical system setup are described in the *Methods*.

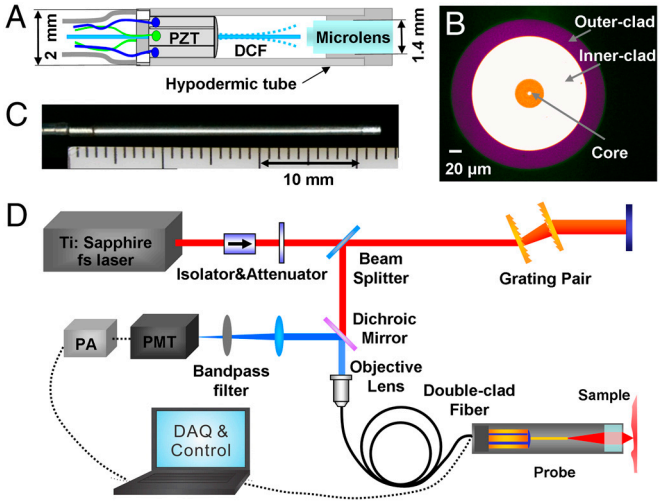

Fig. 1. Optical design of the SHG endomicroscope and the imaging system schematic. (*A*) Schematic of the distal end of the scanning endomicroscope. PZT: tubular piezoelectric actuator; DCF: double clad fiber. (*B*) Photograph of the double-clad fiber cross-section. (*C*) Photograph of the assembled endomicroscope. (*D*) Layout of the endomicroscopy imaging system. PMT: photomultiplier tube; PA: preamplifier; DAQ: data acquisition unit.

Characterization of Endomicroscope Resolution. The high-NA microobjective lens in the endomicroscope enabled us to achieve a small focused spot size and improved lateral resolution by almost twofold over our previously reported systems (16, 20, 21). Fig. 2 shows the two-photon excited fluorescence intensity profile of a 0.1-μm diameter fluorescent bead collected by the endomicroscope along the lateral (Fig. 2*A*) and axial (Fig. 2*B*) direction, respectively. The lateral and axial resolutions of the endomicroscopy system, provided by the full-width-at-half maximum of the Gaussian fit to the respective fluorescence intensity profile, were about 0.76 × 4.36 μm (lateral × axial), which were close to the predicted resolutions of 0.69 × 6.15 μm according to the formula described in ref. 25. The discrepancy is probably attributable to the potential inaccuracy in moving the imaging beam through the small fluorescent bead, a slight lateral position shift (e.g., off the bead center) during the axial scan, and the potential spherical aberration in the microlens.

Performance of SHG Endomicroscope for Cervical Tissue Section Imaging. Mice (C57Bl6/129S) have a gestation time of approximately 19 d with birth occurring early on day 19 (26). Biomechanical

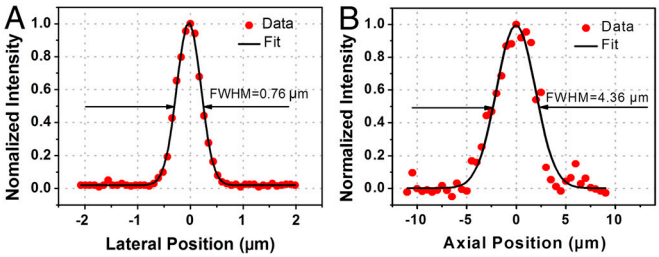

Fig. 2. Endomicroscopy resolution measurements with two-photon excitation. (*A*, *B*) Fluorescence intensity profiles (dots) across the center of a 0.1-μm diameter fluorescent bead along lateral (*A*) and axial (*B*) direction. The fitted Gaussian curves are shown in black traces. The resolution was provided by the corresponding full-width-at-half-maximum (FWHM) of the Gaussian fit.

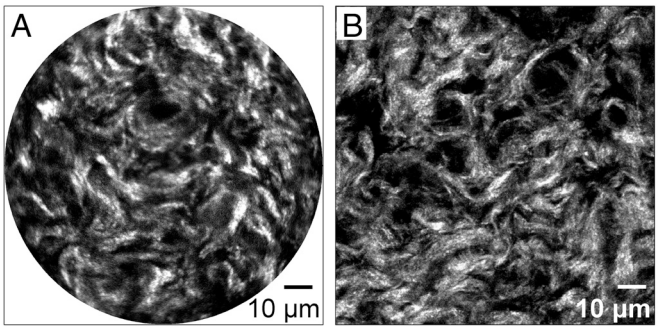

Fig. 3. Representative SHG images of a mouse cervical tissue section at day 18 of gestation acquired with a scanning endomicroscope (*A*) and a bench-top microscope (*B*). The microscopy image was taken with a 20 × 0.95 NA objective with the image size chosen to match endomicroscope field of view. The SHG endomicroscopy image quality is approaching or comparable to the bench-top microscopy.

measurements of cervical tissue identify a progressive increase in tissue compliance that is measurable by day 12 of pregnancy and reaches its maximum at birth (9). The accompanying changes in cervical collagen morphology have been well documented in mouse tissue sections using bench-top SHG microscopy (13). To assess the performance of the SHG endomicroscope, images of frozen sections of cervix from mice at various stages of pregnancy were acquired with the endomicroscope and compared with images of the same tissue section acquired with our bench-top SHG microscope. To allow quantitative comparisons, the SHG imaging conditions were kept constant for all samples. The bench-top SHG microscope is equipped with a 20× 0.95 NA objective lens. The incident power (and temporal pulse width) on the tissue sample was approximately 40 mW (450 fs) and 15 mW (150 fs) for the endomicroscope and microscope, respectively. The imaging speed was 2.7 frames/second with the endomicroscope and 0.37 frames/second for the microscope. Fig. 3*A* shows a representative SHG endomicroscopy image of a cervical section from a mouse at day 18 of gestation, where the fibrillar collagen morphologies can be clearly resolved. The endomicroscope offers a field of view (FOV) of about 110 μm in diameter on the sample. Fig. 3*B* shows the corresponding microscopy SHG image acquired from a similar region with the image size chosen to match the endomicroscope FOV. Considering the differences in the imaging speed, temporal pulse width, incident power, and potential collection efficiency in the two imaging systems, 20 frames and 4 frames were averaged for the endomicroscopy and bench-top microscopy systems, respectively, to achieve a comparable signal-to-noise ratio. These images show that the endomicroscope offered a sufficient excitation and SHG collection efficiency with a resolution approaching a bench-top microscope and image quality sufficient to resolve the fine details of collagen morphology. Image quality is also sufficient to perform 3D imaging by translating the specimen through the focal plane of the endomicroscope with a precision PZT stage. 3D projections of mouse cervical tissue sections on gestation day 15 and day 18 are shown in Fig. S1.

Quantitative Analysis of Collagen Changes During Pregnancy. Fig. 4 shows representative images of cervical sections from nonpregnant (NP) mice and mice at days 6, 12, 15, 18 of pregnancy. SHG microscopy has previously shown that there is a progressive increase in SHG intensity from early to late pregnancy (13) and this was also evident in the endomicroscope data. The contrast of the images in Fig. 4 *A–E* has been adjusted to compensate for intensity differences and optimize visualization of morphological details. The SHG images obtained by endomicroscopy at each stage of pregnancy appeared very similar to those obtained with the bench-top SHG microscope from the same stage of pregnancy, revealing morphological changes of the collagen fiber matrix during pregnancy as reported previously (13). Collagen fibers were highly aligned, thin, and relatively straight in the NP cervix and in early pregnancy (e.g., at day 6 of gestation). The collagen fibers gradually became more curved and thicker in appearance in the later stages of pregnancy. Fig. 4 shows that the progressive changes in morphology of collagen in the SHG images (Fig. 4 *A–E*) correlate generally with images of trichrome stained cervical tissue sections (Fig. 4 *F–J*) at each stage of pregnancy and highlights the power of SHG endomicroscopy to reveal fine details of collagen matrix architecture.

For quantitative analysis of morphology, the images were normalized locally by contrast stretching each image individually to fill an 8-bit grayscale as described in *Methods*. Fig. 5*A* shows that characteristic fiber size increased progressively from NP to day 18 of gestation ($P < 0.0001$ at all time points). In addition, intensity-based analyses were also performed to extract quantitative information such as the fractional area and mean gray value (MGV) of the SHG signals. For these intensity-dependent measurements, the images were normalized globally by adjusting all images at all time points to a fixed grayscale chosen from the minimum and maximum gray values in the aggregate dataset. Different from local normalization, which best reveals the morphological details in each image; the global normalization preserves the relative differences in SHG signal intensity at each time point.

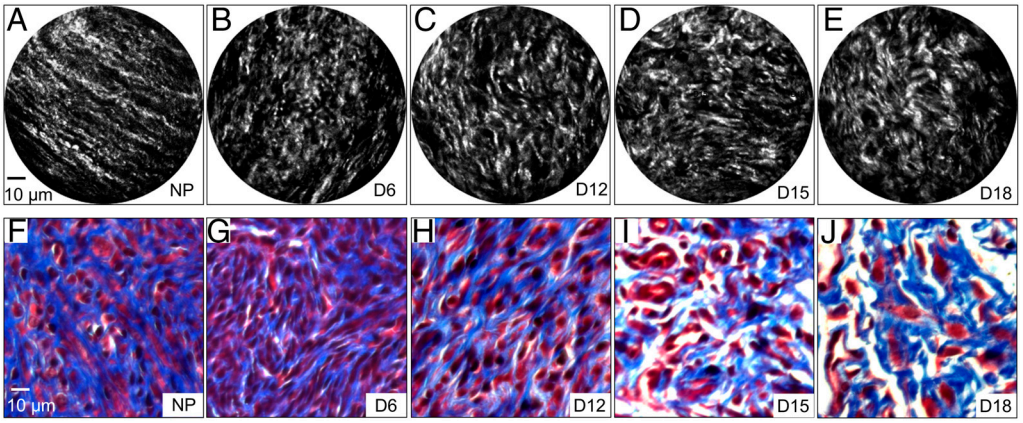

Fig. 4. SHG endomicroscopy images of cervical tissues sections from nonpregnant (NP) (*A*) and pregnant mice at gestation days 6 (*B*), 12 (*C*), 15 (*D*), and 18 (*E*). Significant morphological changes in cervical collagen are evident over the course of pregnancy. Microscopic images of trichrome stained samples (*F–J*) at the same gestational time points show gross changes in collagen morphology.

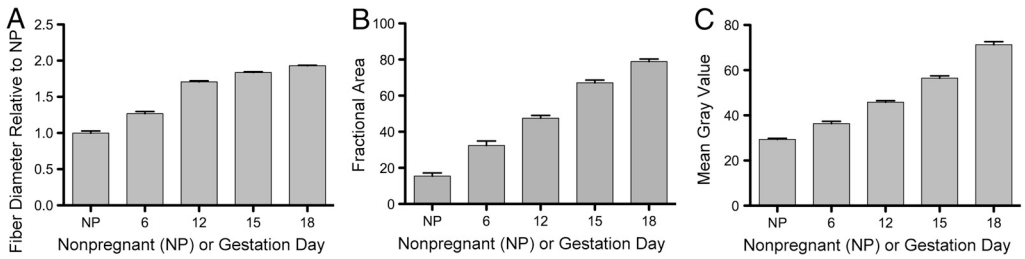

Fig. 5. Quantitative analyses of fiber diameter (*A*), fractional area (*B*) and mean gray intensity (*C*) from endomicroscope images. Features were measured in NP, gestation days 6, 12, 15, and 18 mouse cervical sections. $n = 3$ animals per time point and 25–30 images per animal. All features progressively increased throughout pregnancy. Error bars represent a standard error mean ($P < 0.0001$ for all time points when comparing any two adjacent time points). All time points are significant from one another.

As shown in Fig. 5 *B* and *C*, the resulting fractional area and MGV of the SHG signal above threshold progressively increased throughout pregnancy ($P < 0.0001$ at all time points), reaching a maximum on day 18. These findings confirm that resolution and quality of the endomicroscopy images are sufficient to detect the quantitative changes previously documented only by bench-top SHG microscopy.

Ex Vivo Cervical Tissue Imaging Through Intact Epithelium. In addition to cervical tissue sections, ex vivo mouse cervical tissues (NP and gestation day 18) with intact epithelium were also used for testing the performance of the SHG endomicroscope. Fig. 6*A* shows a photo of an excised NP mouse cervix placed on a wax block. Fig. 6 *B* and *C* show representative SHG endomicroscopy images from NP and day 18 mouse cervical tissue with the probe placed on the outside of the exocervix. Although epithelial cell proliferation during pregnancy leads to an increase in the number of epithelial cell layers, total epithelial thickness is not well documented. Based on our preliminary measurements from multiple NP and gestation day 18 paraffin sections, we observe that the epithelial thickness varies within each time point and ranges from 30 μm to 400 μm thick with an average thickness of about 163 μm. Instead of averaging over 20 frames, only 5 frames of averaging were applied. This reduced the total time to acquire an averaged image from 7.4 s down to 1.85 s. A comparison of image quality based on number of frames averaged is shown in Fig. S2. The SHG endomicroscopy images from mouse tissues through epithelium show similar quality and morphological features as acquired from mouse sections when comparing Fig. 4 *A* and *E* with Fig. 6 *B* and *C*. We further tested the imaging capability of the endomicroscope using human cervical NP and term pregnant specimens with a photo shown in Fig. 6 *D* and *E*, respectively. The representative SHG endomicroscopy images are illustrated in Fig. 6 *F* and *G*. Similar to the mouse cervix, the fine cervical collagen architecture can be clearly observed through the epithelium and the collagen structure clearly changes from long thin collagen fibers in the NP cervix to curved, thicker fibers in term pregnant cervix.

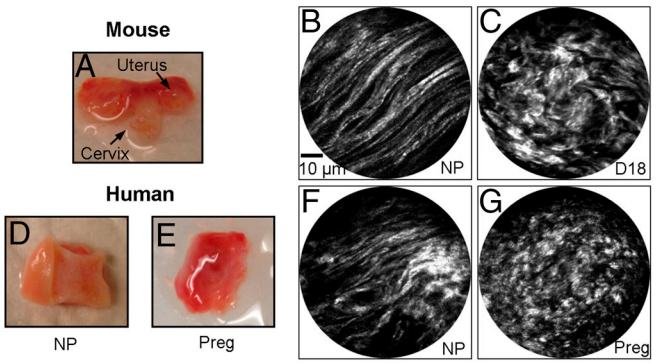

Fig. 6. (*A*) Photo of an excised nonpregnant (NP) mouse cervix placed on a wax block. (*B*) and (*C*) are a representative SHG endomicroscopy image of NP and gestation day 18 mouse cervices, respectively, collected through intact epithelium. The SHG image quality and morphological features are similar to those observed from mouse cervix sections (see Fig. 4 *A* and *E*). (*D*) and (*E*) show photos of cervical specimens from NP and 36-wk pregnant women, respectively, with the exocervix facing up, and a representative SHG endomicroscopy image of these specimens are shown in (*F*) and (*G*), respectively.

Discussion

We have demonstrated the development of a compact fiber-optic SHG endomicroscope capable of collecting SHG images of cervical collagen in tissue sections and ex vivo tissue with intact epithelium. The compact fiber-optic SHG endomicroscope has a resolution and image quality comparable to a bench-top microscope. Compared to previously reported nonlinear optical endomicroscope prototypes (16, 20, 21), our current model offers a significant improvement in signal collection efficiency (i.e., by more than 30-fold), owing to the use of a specially designed DCF with a large SHG collection area and numerical aperture and the introduction of a super achromatic micro-objective lens. The resolution was also improved by almost threefold compared to our first prototype (16), benefiting from the high NA of the micro-objective lens. The choice of a single DCF configuration for excitation laser delivery, SHG signal collection and beam scanning (along with a tubular piezoelectric actuator), made it possible to engineer a scanning endomicroscope with an exceptionally compact footprint. Compared to microelectromechanical system (MEMS)-based probes (17), the current probe configuration does not involve beam folding optics and thus allows for an overall compact probe size. These features will enable future application of SHG endomicroscopy for clinical evaluation of a wide variety of disorders where collagen architecture is altered (27–29). In particular, we propose that translation of this emerging technology into the obstetrics clinic could potentially have a dramatic impact on the understanding and prediction of preterm birth risk. It is envisioned that some parameters of the current endomicroscope originally designed for animal use (such as the probe diameter and rigid length), could be relaxed when intended for human use, offering an opportunity to further improve the imaging performance of the probe (such as a better resolution and a longer working distance). Clinical success with larger multiphoton excitation devices has recently been reported. These devices perform "optical skin biopsies" using both autofluorescence and SHG for diagnosing skin malignancies with no noted adverse effects even at an excitation power about 150 mW (30, 31). This provides further optimism for the clinical potential of this reported endomicroscopy technology.

Alterations in cervical collagen structure and assembly are the earliest identified molecular changes in the cervix during pregnancy and precede measurable biomechanical changes of cervical tissue in mouse models (4, 13). Progressive modification of

collagen architecture is likely to be important for cervical remodeling in women as well, as women with genetic defects that alter collagen processing and assembly (e.g. Ehlers Danlos syndrome) are predisposed to PTB resulting from cervical insufficiency (32, 33). A noninvasive methodology for visualizing changes in cervical collagen organization thus would have the potential to improve diagnosis and treatment in cases where preterm birth involves premature or abnormal remodeling of cervical collagen. Because the SHG signal is an intrinsic property of the assembled collagen fibrils, SHG imaging is ideally suited for visualization of collagen I at the molecular level in vivo without the need for stains or contrast agents. We have shown that the endomicroscope described here has sufficient resolution to distinguish the early changes in cervical collagen architecture during normal pregnancy in mouse tissue and quantify them by image analysis, suggesting the potential clinical application of this methodology for monitoring the progress of pregnancy in women. We have previously shown that SHG microscopy can detect abnormal cervical ripening in a mouse model of preterm birth (4, 13). Application of our SHG endomicroscopy technology to detect aberrations in cervical remodeling in women well in advance of premature birth onset would not only allow early and accurate prediction of PTB risk but also facilitate development of therapies for prevention. Thus, successful translation of this developing technology is likely to have a significant impact on reducing PTB rates, reducing infant mortality rates, and reducing the number of individuals who suffer from the negative lifelong health consequences of prematurity.

Methods

Endomicroscope Probe. The engineering details of the endomicroscope probe can be found in our previous reports (16, 20, 21). In brief, a four-quadrant piezoelectric (PZT) tube was adopted as a cantilever actuator. A double clad fiber was run through and glued to the end of the PZT tube with approximately 1 cm freely standing length as a cantilever, which was actuated by the PZT tube to perform 2-dimensional beam scanning. An open-close spiral-scanning pattern was produced when the two orthogonal pairs of electrodes on the outer surface of the PZT actuator were driven by an amplitude-modulated sine and cosine waves. Effective cantilever tip sweeping was achieved by driving the PZT actuator at or near the mechanical resonant frequency of the fiber cantilever. For a 1-cm long fiber cantilever, the resonant (spiral) scanning frequency was about 1.4 kHz, resulting in an imaging frame rate of about 2.7 frames/second with each frame consisting of 512 spirals. An approximately 500-μm scanning diameter traced by the fiber tip was achieved with a peak-to-peak drive voltage of approximately 50–140 V (depending on the fiber and how well the fiber was attached to the actuator). The corresponding beam scanning range was about 110 μm on the sample when using a compound microlens with a magnification of 0.22. The miniature scanner was housed along with the microlens into a waterproof 14-gauge ultrathin hypodermic tube with an overall outer-diameter of 2 mm and a rigid length of 32 mm.

Endomicroscopy System. Femtosecond pulses generated from a Ti:Sapphire laser (Chameleon Vision II from Coherent Inc.) was tuned to 890 nm with a transform-limited pulse width of approximately 150 fs. The laser has a built-in prechirp unit providing a maximum $-15,000$ fs^2 group velocity dispersion at 890 nm, which can compensate the positive dispersion from a DCF of a length up to 50 cm. Considering the extra length of the DCF in the endomicroscope and other optical components in the beam path (such as a Faraday isolator for preventing the reflections back into the laser, the attenuator for tuning the laser power and lenses for controlling the beam diameter and coupling the beam into the DCF, etc.), which also introduce positive dispersion, a pulse stretcher based on a pair of transmission gratings (600 lines/mm) was employed to provide additional dispersion compensation. The prechirped pulses were launched into the endomicroscope probe through a coupling lens (Olympus 20×0.4 NA objective). The average incident power on the tissue sample was about 40 mW with a measured pulse width of about 450 fs after a 60-cm long DCF in the endomicroscope. The residual pulse broadening was mainly caused by the nonlinear processes in the fiber core, such as self-phase modulation. The SHG signal from the sample was collected by the microlens and then focused back into the DCF. The SHG signal, propagating mainly through the inner clad, was separated at the proximal end of the endomicroscope from the backscattered excitation light by a dichroic mirror (Semrock FF665-Di01), further filtered by a bandpass filter (Semrock FF01-445/20), and then detected by a photomultiplier tube (PMT) (Hamamatsu H7422P). The photo current from the PMT was converted to voltage, amplified, and digitized in synchrony with the PZT actuating waveforms. Polar coordinates were chosen to represent the spiral scan leading to a (r, θ, I_{SHG}) surface where I_{SHG} is the signal intensity measured from the coordinate (r, θ). For storage and analysis, the polar surface was interpolated and mapped onto a two-dimensional Cartesian surface, which was then saved as an eight-bit 1464×1464 pixel image with the range of I_{SHG} being stretched to 256 gray levels.

Animal and Human Tissue Sample Preparation. Mice were housed together overnight and vaginal plugs were checked the next morning. The presence of a vaginal plug was counted as day 0.5 of the 19 day mouse gestation. On days 6, 12, 15, and 18 of gestation, mice were sacrificed and reproductive tissue was removed. Cervical and vaginal tissues were embedded in the optimal cutting temperature (OCT) compound (Tissue Tek, Indiana) and frozen in liquid nitrogen. 50 μm transverse sections were cut and mounted on glass slides. Before imaging, the entire tissue with intact epithelium or the sections were thawed at room temperature and hydrated with phosphate buffered saline. All studies were conducted in accordance with the standards of humane animal care described in the National Institutes of Health Guide for the Care and Use of Laboratory Animals, using protocols approved by an institutional animal care and research advisory committees.

Human cervical tissues from nonpregnant women were obtained at the time of hysterectomy for benign gynecological indications with no cervical pathology. Cervical tissue from a pregnant woman (36 wk) was obtained at the time of cesarean hysterectomy for indications that did not involve cervical pathology. The protocols for human tissue collection are approved by the Institutional Review Board at the University of Texas Southwestern Medical Center. Human samples were cut to include both epithelium and stroma. Tissues were frozen in OCT compound for preservation. Before imaging, the entire tissues were thawed at room temperature and hydrated with phosphate buffered saline, and then placed on the wax block with the exocervix faced outside for imaging.

Trichrome Staining. Mouse cervices were collected and fixed in 4% paraformaldehyde overnight, paraffin embedded and 5-μm sections were cut and stained with Masson's Trichrome as previously described (10). Trichrome staining selectively stains collagen blue and smooth muscle, keratin and cytoplasm pink (34).

Image Analysis. All measurements were preformed on the entire field of view of each image. Fiber diameter measurements were carried out on locally normalized image sets as previously described (13, 35). Briefly, images were analyzed using the FD Math function in ImageJ 1.41k, to obtain the pixel-based intensity autocorrelation over the entire image. A 2-D Gaussian function was fit to the center of the autocorrelation image (excluding the center pixel), and 2 times the standard deviation of the mean was taken as the characteristic fiber size ($n = 3$ animals per time point and 25–30 images per animal). Data for different days of pregnancy were compared using a one-way ANOVA followed by Tukey analysis.

Intensity measurements were carried out on globally normalized images. Day 18 images were used to define a threshold that separated SHG signal from background (i.e., the empty space on the image). Mean gray value (MGV) and fractional area of the pixels above threshold were measured using ImageJ with $n = 3$ animals per time point and 25–30 images per animal. Data were analyzed using a one-way ANOVA followed by Tukey analysis.

ACKNOWLEDGMENTS. The authors would like to acknowledge the assistance of the UT Southwestern Live Cell Imaging Facility, a Shared Resource of the Harold C. Simmons Cancer Center, supported in part by an NCI Cancer Center Support Grant, P30CA142543. We also thank the Human Tissue and Biological Core Laboratory supported by the grant P0111149 and under the directorship of Dr. Ann Word at the University of Texas Southwestern Medical Center for providing human cervical tissue. This research was supported in part by the National Institutes of Health under a Grant R01CA153023 (XL), The Hartwell Foundation (XL and MM), and the Burroughs Welcome Fund (MM).

1. Leppert PC (1995) Anatomy and physiology of cervical ripening. *Clin Obstet Gynecol* 38:267–279.

2. Timmons B, Akins M, Mahendroo M (2010) Cervical remodeling during pregnancy and parturition. *Trends Endocrinol Metab* 21:353–361.

3. Akgul Y, Holt R, Mummert M, Word A, Mahendroo M (2012) Dynamic changes in cervical glycosaminoglycan composition during normal pregnancy and preterm birth. *Endocrinology* 153:3493–3503.
4. Akins ML, Luby-Phelps K, Bank RA, Mahendroo M (2011) Cervical softening during pregnancy: Regulated changes in collagen cross-linking and composition of matricellular proteins in the mouse. *Biol Reprod* 84:1053–1062.
5. Mahendroo M (2012) Cervical remodeling in term and preterm birth: Insights from an animal model. *Reproduction* 143:429–438.
6. Institute of Medicine Committee on Understanding Premature Birth and Assuring Healthy Outcomes (2007) *Preterm Birth: Causes, Consequences, and Prevention* (National Academy of Sciences, Washington, DC).
7. Spong CY (2007) Prediction and prevention of recurrent spontaneous preterm birth. *Obstet Gynecol* 110:405–415.
8. Iams JD, et al. (1996) The length of the cervix and the risk of spontaneous premature delivery. *New Engl J Med* 334:567–572.
9. Read CP, Word RA, Ruscheinsky MA, Timmons BC, Mahendroo MS (2007) Cervical remodeling during pregnancy and parturition: Molecular characterization of the softening phase in mice. *Reproduction* 134:327–340.
10. Holt R, Timmons BC, Akgul Y, Akins ML, Mahendroo M (2011) The molecular mechanisms of cervical ripening differ between term and preterm birth. *Endocrinology* 152:1036–1046.
11. Cox G, et al. (2003) 3-dimensional imaging of collagen using second harmonic generation. *J Struct Biol* 141:53–62.
12. Campagnola PJ, Loew LM (2003) Second-harmonic imaging microscopy for visualizing biomolecular arrays in cells, tissues and organisms. *Nat Biotechnol* 21:1356–1360.
13. Akins ML, Luby-Phelps K, Mahendroo M (2010) Second harmonic generation imaging as a potential tool for staging pregnancy and predicting preterm birth. *J Biomed Opt* 15:026020.
14. Tearney GJ, et al. (1997) In vivo endoscopic optical biopsy with optical coherence tomography. *Science* 276:2037–2039.
15. Gmitro AF, Aziz D (1993) Confocal microscopy through a fiberoptic imaging bundle. *Opt Lett* 18:565–567.
16. Myaing MT, MacDonald DJ, Li XD (2006) Fiber-optic scanning two-photon fluorescence endoscope. *Opt Lett* 31:1076–1078.
17. Fu L, Jain A, Cranfield C, Xie HK, Gu M (2007) Three-dimensional nonlinear optical endoscopy. *J Biomed Opt* 12:040501.
18. Flusberg BA, Lung JC, Cocker ED, Anderson EP, Schnitzer MJ (2005) In vivo brain imaging using a portable 3.9 gram two-photon fluorescence microendoscope. *Opt Lett* 30:2272–2274.
19. Bao HC, Allen J, Pattie R, Vance R, Gu M (2008) Fast handheld two-photon fluorescence microendoscope with a 475 μm × 475 μm field of view for in vivo imaging. *Opt Lett* 33:1333–1335.
20. Wu YC, Leng YX, Xi JF, Li XD (2009) Scanning all-fiber-optic endomicroscopy system for 3D nonlinear optical imaging of biological tissues. *Opt Express* 17:7907–7915.
21. Wu YC, Xi JF, Cobb MJ, Li XD (2009) Scanning fiber-optic nonlinear endomicroscopy with miniature aspherical compound lens and multimode fiber collector. *Opt Lett* 34:953–955.
22. Murari K, et al. (2011) Compensation-free, all-fiber-optic, two-photon endomicroscopy at 1.55 um. *Opt Lett* 36:1299–1301.
23. Rivera DR, et al. (2011) Compact and flexible raster scanning multiphoton endoscope capable of imaging unstained tissue. *Proc Natl Acad Sci USA* 108:17598–17603.
24. Liu XM, Cobb MJ, Chen YC, Kimmey MB, Li XD (2004) Rapid-scanning forward-imaging miniature endoscope for real-time optical coherence tomography. *Opt Lett* 29:1763–1765.
25. Zipfel WR, Williams RM, Webb WW (2003) Nonlinear magic: Multiphoton microscopy in the biosciences. *Nat Biotechnol* 21:1369–1377.
26. Murray SA, et al. (2010) Mouse gestation length is genetically determined. *PLoS One* 5:e12418.
27. He Y, et al. (2010) Toward surface quantification of liver fibrosis progression. *J Biomed Opt* 15:056007.
28. Zheng L, et al. (2011) Label-free discrimination of normal and fibroadenomal breast tissues using second harmonic generation imaging. *Scanning* 33:208–210.
29. Campagnola P (2011) Second harmonic generation imaging microscopy: Applications to diseases diagnostics. *Anal Chem* 83:3224–3231.
30. Konig K, Riemann I (2003) High-resolution multiphoton tomography of human skin with subcellular spatial resolution and picosecond time resolution. *J Biomed Opt* 8:432–439.
31. Chen SY, Wu HY, Sun CK (2009) In vivo harmonic generation biopsy of human skin. *J Biomed Opt* 14:060505.
32. Petersen LK, Uldbjerg N (1996) Cervical collagen in non-pregnant women with previous cervical incompetence. *Eur J Obstet Gynecol Reprod Biol* 67:41–45.
33. Anum EA, Hill LD, Pandya A, Strauss JF (2009) Connective tissue and related disorders and preterm birth: Clues to genes contributing to prematurity. *Placenta* 30:207–215.
34. Woods GL, Walker DH (1996) *Laboratory Histopathology, a Complete Reference* (Churchill Livingston Press, New York).
35. Raub CB, et al. (2008) Image correlation spectroscopy of multiphoton images correlates with collagen mechanical properties. *Biophys J* 94:2361–2373.